Design of a crash energy absorber for a composite aircraft fuselage using a combined analytical–numerical approach

Poorte, Victor K.; Bisagni, Chiara

DOI
10.1007/s13272-024-00787-x

Publication date
2024

Document Version
Final published version

Published in
CEAS Aeronautical Journal

CEAS Aeronautical Journal
https://doi.org/10.1007/s13272-024-00787-x

ORIGINAL PAPER

Design of a crash energy absorber for a composite aircraft fuselage using a combined analytical–numerical approach

Victor K. Poorte[1] · Chiara Bisagni[1,2]

Received: 6 May 2024 / Revised: 27 September 2024 / Accepted: 28 October 2024

Abstract
To improve the crashworthiness design of composite aircraft structures, analytical models are useful to enable engineers to have a fundamental understanding of the influence of the design variables. As such, during the preliminary design, this knowledge can be exploited, rather than needing to alter an already mature design in a later phase. Accordingly, an analytical model is derived which allows the determination of the mean crushing load and the energy absorption of composite absorbers. The analytical model allows one to accurately predict the mean crushing load of square tube absorbers while altering their side length and thickness. Moreover, the different terms in the analytical model show that the out-of-plane shearing of the material is the major energy dissipating phenomenon. The composite absorbers are then incorporated into a finite element model of the keel section of the thermoplastic composite subfloor of a fuselage demonstrator developed by the Clean Sky 2 STUNNING project. The analytical model facilitates the estimation of the energy absorption and crash load of the fuselage section augmented with the energy absorbers. In this way, during the preliminary design, the absorbers of the fuselage can be designed concurrently for the static loads and for the crash loading, leading to a more efficient design.

Keywords Aircraft fuselage design · Composite structure · Crashworthiness · Analytical model · Finite element analysis · Thermoplastic

1 Introduction

The aviation industry is well-known for its safety standards, leading it to be one of the safest transport sectors. One major aspect of safety is the crashworthiness of the aircraft, which is the ability of the structure to handle crash loading. Crashworthiness requirements are reported in the Airworthiness Standards [1], which mainly define the maximum accelerations the passengers may experience, the maintenance of livable volume, and constraints for all objects in the cabin, to ensure that the passengers are able to exit the aircraft in the event of a crash. Nowadays, crashworthiness analysis is usually performed at the end of the design cycle when the final design of most of the components is already defined. Consequently, if needed, mature designs have to be altered to account for the additional requirements. Analytical models can help in performing fast crashworthiness analysis during the preliminary stages, leading to more synergistic designs.

Fiber-reinforced polymers show different failure modes when subjected to crush loading, mainly consisting of progressive folding, progressive splaying and progressive fragmentation [2]. The folding failure mode is more common when using ductile materials [3], while the fragmentation and splaying failure modes are more common in the case of more brittle materials. Generally, a combination of the two brittle failure modes occurs, depending on the design of the absorber. Due to the complex failure mechanics of composite energy absorbers, physical testing is the most common way of determining the performance [4]. Falzon addresses the complexity of modeling the crushing behavior, highlighting the complexity of capturing nanocracks mechanics in a macroscale crushing [5]. To capture the splaying and delamination of the crushing, multi-layer finite element methods have been suggested [6–9]; however, the simulation of these models can be time-consuming, due to the high number of degrees of freedom, especially when these are

✉ Chiara Bisagni
c.bisagni@tudelft.nl

1 Faculty of Aerospace Engineering, Delft University of Technology, Kluyverweg 1, Delft 2629 HS, The Netherlands

2 Department of Aerospace Science and Technology, Politecnico di Milano, Via La Masa 34, Milano 20156, Italy

incorporated in structural models. A method to capture the crushing phenomenon using single shell models is shown in [8, 10, 11], to reduce the computation effort for a single absorber. More recent work by Costa et al. focuses on developing a physically based finite deformation model, which captures the complex failure behavior of the matrix and kinking of the fibers [12]. While finite element models can capture the crash behavior of isolated elements and articulate structures, the creation and simulation time of the models is time-consuming. Moreover, to capture the complex failure behavior of fiber-reinforced plastics, the material models need to be validated with physical tests, which once more is a costly procedure.

In literature, different approaches can be found that aim to analytically determine the mean crushing load of composite absorbers. The most accurate methods consider the energy dissipations of the various failure modes that are exhibited during the crushing phenomenon [13, 14]. However, the applicability of energy dissipation is limited as it requires the use of load cycles, which are difficult to determine. This problem is overcome by Hussein et al. [14], who introduced the use of energy rates in combination with the loading rates. The equation to determine the mean crushing load as derived by Hussein et al. is applicable to straight square tubes.

Next to the analysis of single structural elements, the behavior of more complex structures is also subject in recent studies [15–18], but most of them consider metal structures. Sub-floors contribute to a large part of the energy absorption [19]. For example, the bending of metal frames entails almost half of the total energy absorption [20]. The crash behavior is sometimes studied by performing physical tests, by dropping a section of the fuselage [21, 22], while [23, 24] show how finite element modeling aids in the crashworthiness analysis of aircraft structures. Including crash requirements during the aircraft's preliminary design can be challenging, but improves the design [25]. The crash kinematics may change when implementing fiber-reinforced materials. This leads to the investigation of different types of energy absorption systems, leveraging the properties of composites [26]. As such it should be studied how composite aircraft behave when subjected to crash loading, to ensure that these are in line with regulation [27, 28].

This study develops a simplified analytical–numerical approach which models the crushing behavior of composite energy absorbers and subsequently estimates the crashworthiness behavior of the keel section of an aircraft fuselage. This is done by further developing existing analytical methods to determine the mean crushing load of composite energy absorbers and providing an approach to model the crash behavior of thermoplastic composite aircraft structures. By doing so, direct insight is achieved into the design variables that influence the fuselage crashworthiness performance, limiting the need for time consuming computer simulations. The method enables one to perform quick design iterations in the preliminary stage of the aircraft structure, increasing the effectiveness of the design process.

2 Analytical–numerical approach

The developed methodology comprises three parts, which are described in this section. First, an analytical model is derived. Afterward, the finite element model of the crush energy absorber, required for verifying the analytical model, is considered. Finally, the fuselage section is modeled, taking into account the interaction between the different parts, which is key in achieving the desired crash kinematics.

2.1 Analytical model

The analytical model here developed is based on the work of Hussein et al. [14] and focuses on the energy dissipating phenomena that occur during the crushing of a tube. The energy-dissipating phenomena are the formation of vertical splits, fragmentation, friction between the strut and the crushing plate, and central wall delamination. The crush frond geometry investigated in this study is similar to the one assumed by Hussein et al. [14], with the addition of the taper angle of the specimen, as reported in Fig. 1. This enables the study of conical or pyramid-like shapes. By introducing the taper angle into the model, one can relate the loading velocity to the loading rate the sidewall of the specimen experiences, which dictates the rate at which the material is fed into the crush frond. The velocity is obtained with the relation reported in Eq. 1, where v_c is the velocity the specimen's sidewall experiences, while v is the actual crushing velocity; finally, ϕ is the sidewall's taper angle.

$$v_c = v / \cos \phi \tag{1}$$

The mean crushing load can be determined by setting up the energy balance between the rate at which the energy is being put into the system and the rate at which the energy is absorbed. The energy rate being put into the system is a function of the mean crushing load, whereas the absorption rate is given by the sum of all the material failures as well as of the friction. As such, the single energy rates have to be determined, yielding the mean crushing load upon rearranging.

The delamination energy rate ($\dot{W}_{c1}$) can be derived using the Mode I fracture toughness of the material (G_{IC}) and the surface area rate at which the delamination propagates ($\dot{A}$), as depicted in Eq. 2. The delaminating area rate can be written as a function of the perimeter of the composite element and the feed rate of the crush frond, denoted with p and v_c, respectively. Finally, the loading rate of the crush frond is

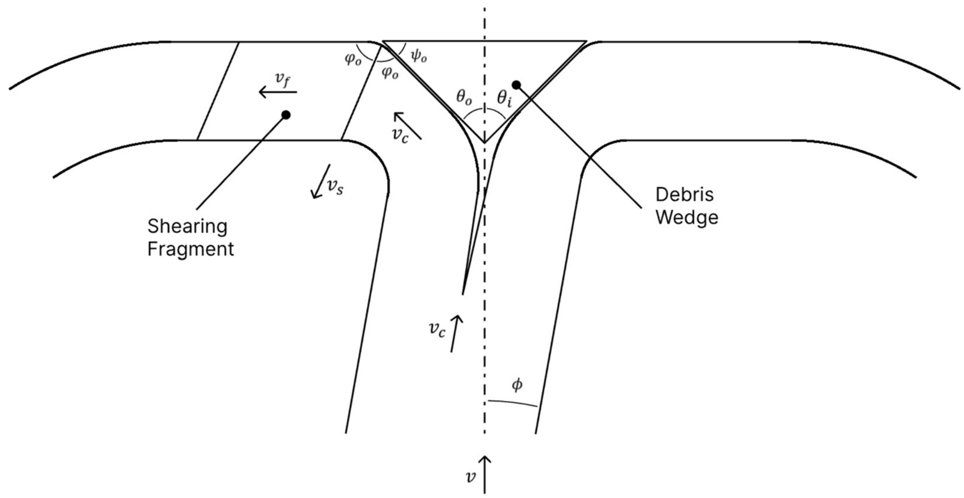

Fig. 1 Idealized crush frond geometry

written as a function of the load rate of the specimen, holding the last form of Eq. 2. The effect of Mode II delamination is assumed to be negligible.

$$\dot{W}_{c1} = G_{IC}\dot{A} = G_{IC}pv_c = \frac{G_{IC}p}{\cos\phi}v \tag{2}$$

The rate of vertical splitting energy ($\dot{W}_{c2}$) is given by the product between the energy released per volume fraction of the material and the failing volume rate [14]. The energy release is determined by simplifying the behavior of the laminate with a linear relation, where the energy is given by the area under the stress–strain curve, thus half the product between the failure stress and strain of the material, denoted with $\sigma_{u,22}$ and $\varepsilon_{u,22}$. The failure stress and strain are taken in the transverse 22 direction, 90° direction in Subfigure 2a, as the splits form in the axial direction of the absorber, and the longitudinal 11 direction of the laminate is assumed to be in line with the axis of the absorber, 0° direction in Subfigure 2a. The volume rate is, on the other hand, given by the failing volume of a single split ($\dot{V}$), which is then multiplied by the number of splits (n). The number of splits corresponds to the corners in the cross section, where stress concentrations cause failure [14]. For round cross sections, determining the number of splits is not possible. However, as we will later demonstrate, this does not pose an issue for implementing the model. The single split failing volume rate is given by the product between the thickness of the laminate (t), the length of the split (l), and the loading rate of the split (v_c). The different derivation steps are reported in Eq. 3.

$$\dot{W}_{c2} = \frac{1}{2}\sigma_{u,22}\varepsilon_{u,22}n\dot{V} = \frac{1}{2}\sigma_{u,22}\varepsilon_{u,22}ntlv_c = \frac{n\sigma_{u,22}\varepsilon_{u,22}tl}{2\cos\phi}v \tag{3}$$

The rate of the out-of-plane shearing energy is given by the product between the force required to push the fragments outward (F_s) and the associated rate (v_s). In turn, the load is obtained using the out-of-plane failure stress of the laminate (τ_s), and the surface area of the failure (A_s). The result of this is depicted in Eq. 4. The equation shows that two components contribute to the energy dissipation, namely the inward and outward splaying layers, indicated with the subscripts i and o, respectively.

$$\dot{W}_s = F_s v_s = A\tau_s v_s = \left(A_{s,i}v_{s,i} + A_{s,o}v_{s,o}\right)\tau_s \tag{4}$$

The failure rate of Eq. 4 is rewritten as a function of the actual loading rate and the material debris angle, denoted with θ. The failure area is the product of the perimeter of the specimen (p), which is assumed to be constant for both the inward splaying and outward splaying layers, and the splaying thicknesses (t_i and t_o), where i and o indicate once more the inward and outward splaying layers.

$$\dot{W}_s = \left(\frac{t_i v_{s,i}}{\sin\varphi_i} + \frac{t_o v_{s,o}}{\sin\varphi_o}\right)p\tau_s = \left(\frac{\cos\theta_i}{\sin^2\varphi_i}t_i + \frac{\cos\theta_o}{\sin^2\varphi_o}t_o\right)p\tau_s v_c \tag{5}$$

The common terms for the inwards and outwards splaying layers are grouped to obtain a more compact form for the out-of-plane shearing energy contribution, yielding Eq. 6.

$$\dot{W}_s = \left[\frac{\cos\theta_i}{\sin^2\left(\frac{\pi}{4}+\frac{\theta_i}{2}\right)}t_i + \frac{\cos\theta_o}{\sin^2\left(\frac{\pi}{4}+\frac{\theta_o}{2}\right)}t_o\right]\frac{p\tau_s}{\cos\phi}v \tag{6}$$

The frictional energy rate ($\dot{W}_f$) is a function of the rate at which the crushing frond slides along the crushing plate, which is equal to the rate at which the material is fed into the crush frond, the normal force (P), and the friction coefficient (μ). The crush frond feed rate is rewritten as a function of the crush rate, which yields the final form in Eq. 7.

Table 1 Material properties of IM7/8552 unidirectional composite lamina

Variable	Symbol	Value	Unit
Mass density	ρ	1.58E-06	kg/mm^3
Young's modulus - Fiber direction	E_{11}	165000	MPa
Young's modulus - Traverse direction	E_{22}	9000	MPa
Shear modulus	G_{12}, G_{31}	5600	MPa
Shear modulus	G_{23}	2800	MPa
Poisson ratio	ν_{12}	0.0185	-
Tensile strength - Fiber direction	X^T	2560	MPa
Compressive strength - Fiber direction	X^C	1590	MPa
Tensile strength - Traverse direction	Y^T	73	MPa
Compressive strength - Traverse direction	Y^C	185	MPa
Shear strength	S^L	90	MPa
Tensile failure strain - Fiber direction	ε_{11}^T	0.01551	mm/mm
Compressive failure strain - Fiber direction	ε_{11}^C	0.011	mm/mm
Tensile failure strain - Traverse direction	ε_{22}^T	0.0081	mm/mm
Compressive failure strain - Traverse direction	ε_{22}^C	0.032	mm/mm
Engineering failure shear strain	γ_{12}	0.05	mm/mm

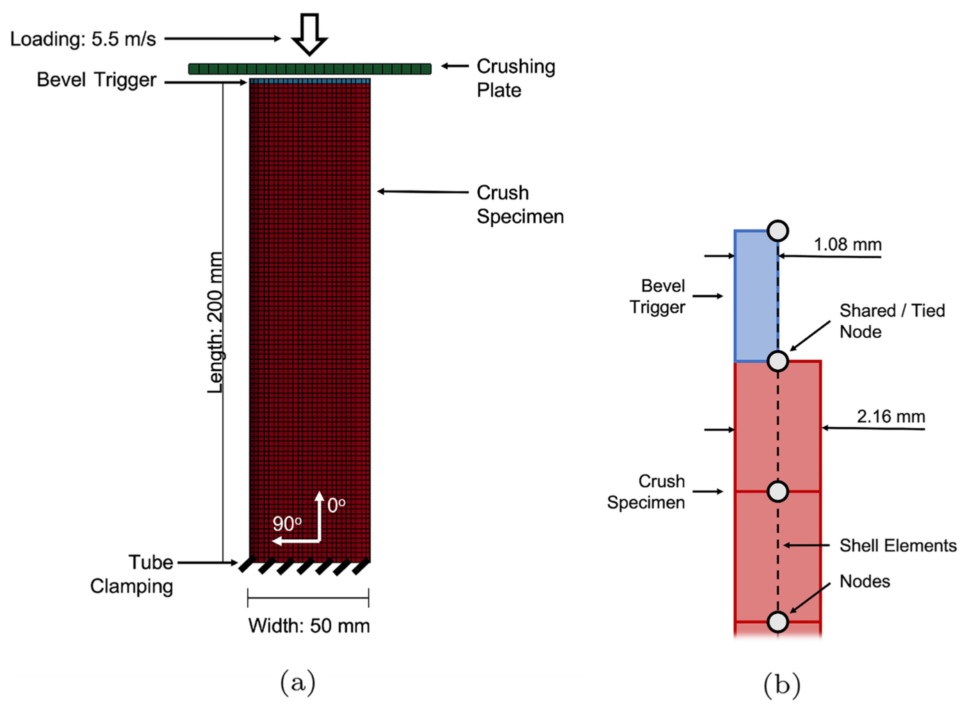

Fig. 2 Square tube: **a** finite element model, **b** detail of the modeled trigger

$$\dot{W}_f = P\mu v_c = \frac{P\mu}{\cos\phi}v \tag{7}$$

Equation 8 is obtained imposing equilibrium, grouping all the energy dissipations on the right-hand side of the equation and the in-going energy, given by the load (P) multiplied by the actual crushing velocity (v), on the left-hand side.

$$Pv = \frac{G_{IC}p}{\cos\phi}v + \frac{n\sigma_{u,22}\varepsilon_{f,22}tl}{2\cos\phi}v + \left[\frac{\cos\theta_i}{\sin^2\left(\frac{\pi}{4}+\frac{\theta_i}{2}\right)}t_i + \frac{\cos\theta_o}{\sin^2\left(\frac{\pi}{4}+\frac{\theta_o}{2}\right)}t_o\right]\frac{p\tau_s}{\cos\phi}v + \frac{P\mu}{\cos\phi}v \tag{8}$$

First, the common v term can be removed from all the terms. Afterward, the equation can be rearranged, which leads to the final equation of the mean crushing load P as reported in Eq. 9.

$$P = \frac{\frac{G_{IC}p}{\cos\phi} + \frac{n\sigma_{u,22}\varepsilon_{f,22}tl}{2\cos\phi} + \left[\frac{\cos\theta_i}{\sin^2\left(\frac{\pi}{4}+\frac{\theta_i}{2}\right)}t_i + \frac{\cos\theta_o}{\sin^2\left(\frac{\pi}{4}+\frac{\theta_o}{2}\right)}t_o\right]\frac{p\tau_s}{\cos\phi}}{1-\frac{\mu}{\cos\phi}} \tag{9}$$

2.2 Finite element model of the energy absorber

The finite element models of composite square tubes are developed in LS-Dyna to analyze the crushing behavior and verify the analytical model. However, as the numerical models themselves also need validation, the first modeled tube is equal to the 46b and 47B specimens tested by the Oak Ridge National Laboratory (ORNL) [29]. Later, the side length and thickness of the tube are changed to investigate different configurations.

The ORNL test specimen is a square tube of length 200 mm and a side length of 50 mm while having a 6.4 mm mid-plane corner radius. The material is Hexcel IM7/8552, which properties are reported in Table 1 [29]. A quasi-isotropic layup is used, $[0_2/\pm 45/90_2]_s$ with total thickness of 2.16 mm. In the test, the tube is impacted with a drop weight, meaning that the loading speed of the tube varies in time. By analyzing the first 16 ms, it is found that a constant impact velocity of 5.5 m/s is an accurate approximation [11]. Accordingly, this impact speed and simulation time were selected for the simulation.

The side length of the tubes is then easily changed, while the thickness is altered changing the thickness of the plies in the model. Naturally, this would not be possible in real scenarios as the thickness of a single ply can not be easily changed; nevertheless, this modeling technique is selected for simplicity.

Two approaches can be adopted when modeling the crushing of composite specimens. One method uses a single element through the thickness of the specimen [8, 10, 11], while other methods use multiple elements, each representing a single lamina, which are connected using cohesive elements [6, 7, 30]. The latter method provides more insight regarding delamination in the specimen, but the computational effort is much higher, and therefore deemed unfeasible when studying a large structure, such as a full fuselage section. Accordingly, the model with a single element through the thickness is implemented.

In reference research, where a square tube with similar dimensions is studied, a mesh sensitivity study is performed where it is found that a mesh size of 5 mm is satisfactory [31]. The tube is meshed using a seed of 2 mm, using ELFORM 2 elements. By doing so, 9200 elements are obtained.

The orientation of the laminate is based on the orientation of the shell elements, to guarantee the proper orientation of the lamina when large deformations in the crush zone occur, and during the removal of elements when these fail [32].

Next to the tube itself, a rigid mass is modeled which represents the crushing plate. The movement of the plate is restricted in all directions but the axial direction of the tube, is modeled to move at a constant rate of 5.5 m/s. The total simulation time is set to 16 ms. The lower nodes of the tube are constrained in all degrees of freedom.

The inclusion of bevel triggers is key to ensure the formation of a stable crush frond [2]. While recent research studies different shapes of bevel triggers [33], in the physical test, a 45° bevel trigger is used, to promote the formation of a stable crush frond. It must thus be noted that this angle is different from the taper angle of the specimen's geometry. Therefore, the bevel is modeled in LS-Dyna as a separate part. The thickness of the bevel is halved by omitting the symmetry of the laminate. Subsequently, the two parts are connected by sharing the lower nodes of the bevel and the upper nodes of the tube. Figure 2a depicts the finite element model of the whole tube, while in Fig. 2b, a detail of the bevel trigger is reported.

Contacts are defined as prescribed by the LS-Dyna User Manual [34] for crash simulations. As such, the finite element code automatically detects whether parts are in contact or when a part comes into contact with itself. Literature reports a large scatter of friction coefficients, with values going from 0.1 up to 0.6 [7, 35, 36]. Determining the proper friction coefficient is challenging. In the work presented by Cherniaev et al., a similar tube is modeled, where a friction coefficient of 0.2 is used [11].

In this study, the MAT_LAMINATED_COMPOSITE_FABRIC (MAT058) material model is used. An important aspect of such models is the numerical material parameters, which need to be calibrated with test data. These variables mainly entail stress limits, the time-step limit, and the crush frond softening factor. The calibrated material values are summarized in Table 2. Most of the variables are taken as suggested by the LS-Dyna user manual, while others are calibrated to match the test data, or are based on the work of Cherniaev et al. (2018) [11].

In addition to the material card, other cards are used to control the stability and quality of the simulation:

- CONTROL_TIMESTEP: The steps size is limited to 0.5 to increase the accuracy of the simulation. This cannot be reduced too much, to secure the validity of the simulation, as well as not to increase the computational effort.
- CONTROL_HOURGLASS: IHQ is set equal to 4, to reduce the hourglassing of the elements. When using this

Table 2 Numerical MAT058 card values

Variable	Symbol	Value	Unit	Source
Maximum effective strain for element failure	ERODS	−0.55	mm/mm	[11]
Stress limit fibers tension	SLIMT1	0.01	MPa/MPa	[34]
Stress limit fibers compression	SLIMC1	0.375	MPa/MPa	[11]
Stress limit matrix tension	SLIMT2	0.1	MPa/MPa	[34]
Stress limit matrix compression	SLIMC2	1.0	MPa/MPa	[34]
Stress shear	SLIMCS	1.0	MPa/MPa	[34]
Element time-step limit	TSIZE	1.0E-07	s	[11]
Crush frond softening factor	SOFT	0.57	–	[11]

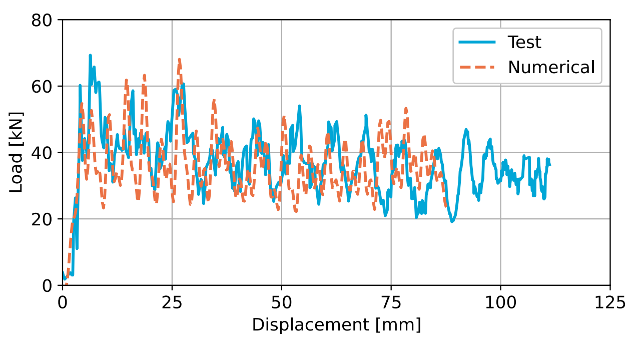

Fig. 3 Comparison between the crushing load of the numerical analysis and the test data

setting, the hourglassing of the parts needs to be below 10% of the part's total energy.

- CONTROL_ACCURACY: The laminate's orientation is based upon the numbering of the nodes of the shell. Therefore, when elements are removed from the simulation, the correct renumbering needs to be ensured. To achieve this, the invariant mode is activated by setting INN equal to four.
- MAXINT: The number of integration points through the thickness of the shell element needs to be altered in the DATABASE_EXTEND_BINARY card, based on the number of layers of the laminate.
- LAMSHT: The flag needs to be activated in the CONTROL_SHELL card, to enable variable strain through the thickness of the laminate, to accommodate bending in the shell.

Figure 3 reports the load as obtained from the simulation, compared to the tests reported in [29]. The crushing load is extracted from the simulation using the CONTACT_FORCE_TRANSDUCER_PENALTY_ID card, and subsequently filtered using the built-in low-pass digital filter (SAE), with a cut-off frequency of 1000 Hz [37]. The plot shows that there is a good correlation between test and simulation data, meaning that the chosen material parameters are satisfactory.

Figure 4 depicts the obtained deformation at three different time instances of the simulation. It is characterized by a combination of splaying and fragmentation.

When using an Intel i5-4670 core, running at 3.40 GHz, with a RAM of 8.00 GB, the CPU time for the crush simulation is of 3 h, and 48 min.

Fig. 4 Deformed states of the crushing of the square tube: **a** time = 5.3 ms, displacement = 29.2 mm, **b** time = 10.6 ms, displacement = 58.3 mm, **c** time = 16.0 ms, displacement = 88.0 mm

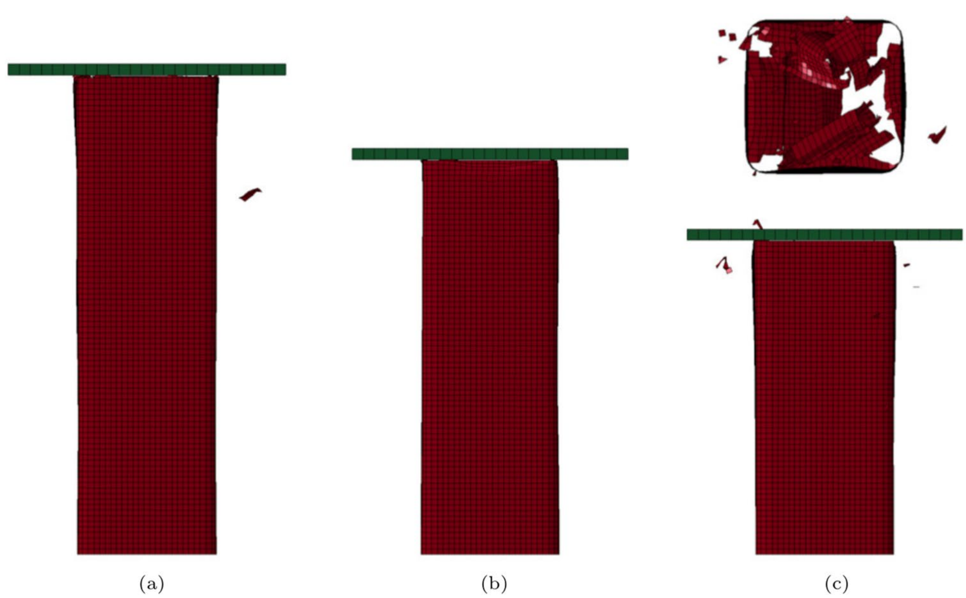

2.3 Finite element model of the fuselage structure

In the previous section, an isolated crush absorber has been studied. This has been done to analyze the crushing behavior of such a tube in a controlled environment and gain insight into the material model. In this section, the absorber is integrated into the keel section of the Next-Generation Multifunctional Fuselage Demonstrator developed by the Clean Sky 2 STUNNING project. The studied fuselage is manufactured in thermoplastic composite material and is characterized by a traditional skin, stringers and frame configuration. The computational effort is reduced by only simulating the keel section of the fuselage. This is achieved by making a cut above the cargo cross-beam, and considering only two frame sections, as shown in Fig. 5. In the figure, one can note two sets of C-struts situated between the cargo crossbeam and the fuselage frames. These serve as supporting struts for the cargo beams; however, the current study investigates how these C-struts perform in the event of a crash.

The crash behavior of the fuselage is modeled in LS-Dyna's finite element code, and the knowledge of the material models gained in the isolated crush simulations can be implemented during the modeling of the fuselage section.

The crash is modeled with a rigid plate, which moves upwards at a constant rate of 10 m/s, recreating the downwards motion of the fuselage. This rate is based on the required impact velocity as reported by the Transport Aircraft Crashworthiness and Ditching Working Group [38]. To limit the upper and sideways movement of the fuselage, the nodes along the cutting line used to obtain the lower section, are fixed in all degrees of freedom.

The structure is modeled using ELFORM 2 elements with the material's behavior characterized with the MAT058 material model.

The studied fuselage section is manufactured using Toray Cetex TC1225 thermoplastic material, in which properties are reported in Table 3 [39].

As the material of the fuselage section is different from the previously described simulations, the numerical variables need to be changed. Ideally, one would calibrate the numerical material parameters with test data. However,

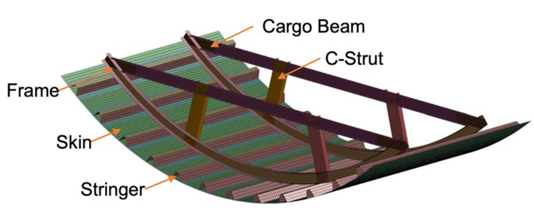

Fig. 5 Fuselage demonstrator section

Table 4 Toray Cetex TC1225 numerical material properties

Variable	Symbol	Value	Unit
Stress limit fibers tension	SLIMT1	0.01	MPa/MPa
Stress limit fibers compression	SLIMC1	0.6	MPa/MPa
Stress limit matrix tension	SLIMT2	0.1	MPa/MPa
Stress limit matrix compression	SLIMC2	1.0	MPa/MPa
Stress shear	SLIMCS	1.0	MPa/MPa
Element time-step limit	TSIZE	1.0E-07	s
Effective failure strain	ERODS	−0.55	mm/mm

Table 3 Toray Cetex TC1225 material properties [39]

Variable	Symbol	Value	Unit
Mass density	ρ	1.59E-06	kg/mm^3
Ply thickness	t_{ply}	0.184	mm
Young's modulus - Fiber direction	E_{11}	143000	MPa
Young's modulus - Traverse direction	E_{22}	8800	MPa
Shear modulus	G_{12}, G_{31}	4300	MPa
Shear modulus	G_{23}	3400	MPa
Poisson ratio	ν_{12}	0.0185	-
Tensile strength - Fiber direction	X^T	2755	MPa
Compressive strength - Fiber direction	X^C	1089	MPa
Tensile strength - Traverse direction	Y^T	78	MPa
Compressive strength - Traverse direction	Y^C	248	MPa
Shear strength	S^L	48	MPa
Tensile failure strain - Fiber direction	ε_{11}^T	0.019	mm/mm
Compressive failure strain - Fiber direction	ε_{11}^C	0.008	mm/mm
Tensile failure strain - Traverse direction	ε_{22}^T	0.009	mm/mm
Compressive failure strain - Traverse direction	ε_{22}^C	0.028	mm/mm
Engineering failure shear strain	γ_{12}	0.05	mm/mm

due to the lack of test data, the values as suggested by the LS-Dyna user manual are adopted. They are reported in Table 4.

All the parts of the fuselage section are made of composite materials, apart from the plates connecting the cargo beams to the frames, which are in AA6111-T4 aluminum alloy. The material properties of the aluminum alloy are reported in Table 5.

The simulation is stabilized by including the same cards used in studying the energy absorber. However, the time-scaling factor is increased from 0.5 to 0.75, to alleviate the computational effort; while an average friction coefficient is taken with respect to references [7, 35], leading to a static friction coefficient of 0.15 and a dynamic coefficient of 0.08, to be conservative.

An important aspect is the connection between the parts. In the actual fuselage, the parts are welded together [40]. The stringers are conduction welded to the skin [41]. Ideally, the failure of the connection between the parts should be modeled; however, it would drastically increase the computational effort. Consequently, the parts connections are fixed, connecting one part's nodes to the surface of the neighboring part.

As no test data is available to validate the finite element model, the energies within the different parts are used to evaluate the quality of the simulation. When doing so, one must ensure that there is little hourglassing energy in the single parts and that the energy ratio is close to one [34].

3 Results

This section presents the results of the analytical–numerical approach. First, the ability of the analytical model to estimate the mean crushing load of the composite energy absorber is studied. Afterward, the performance of the keel section of the fuselage is analyzed, where it is seen how different geometries of absorbers behave when integrated into the structure. Finally, the suggested method is summarized, showing how the synergy between the analytical and numerical models can aid during the preliminary design process.

Table 5 AA6111-T4 material properties

Variable	Symbol	Value	Unit
Mass density	ρ	2.89E-06	kg/mm^3
Young's modulus	E	70500	MPa
Poisson ratio	ν_{12}	0.34	-
Yield stress	σ_y	192.1	MPa

Table 6 Analytical and numerical mean crushing load for varying side lengths of the square tube

Specimen	Mean Crushing Load	
Side Length	Num.	An.
[mm]	[kN]	[kN]
25	18.0	18.0 (0.0%)
35	25.8	26.1 (1.2%)
50	36.2	38.2 (5.5%)
65	45.9	50.3 (9.6%)
75	37.6	58.4 (55.3%)

3.1 Energy absorber

Tables 6 and 7 report the mean crushing load as obtained from the finite element simulation and the analytical model, along with the relative difference as a percentage, for different side lengths or thicknesses of the square tube. When varying the side length, a thickness of 2.16 mm is used; while, when varying the thickness, a side length of 50 mm is used. It can be seen that there is a good correlation between the numerical and the analytical results, denoted by the small percentage difference between the two loads. Exceptions to this are the tubes with small thickness and large side length. The discrepancy can be attributed to the geometric instability that arises with these dimensions, leading to the collapse of the absorber, and thus a loss in load-carrying capability.

The analytical model is able to capture the variation of the mean crushing load changing the side length and thickness, allowing a quick estimation of the energy absorption and reducing the need for timely finite element simulations.

To further study the analytical model, Table 8 reports the values computed for the different energy-dissipating phenomena. This enables understanding the contribution of every failure phenomenon on the total energy dissipation. The reported values are those obtained from the tube with a side length of 50 mm and thickness of 2.16 mm. The contribution of every energy-dissipating phenomenon is

Table 7 Analytical and Numerical mean crushing load for varying thicknesses of the square tube

Specimen	Mean Crushing Load	
Thickness	Num.	An.
[mm]	[kN]	[kN]
1.08	3.4	19.2 (464.7%)
1.62	21.3	28.7 (34.7%)
2.16	36.2	38.2 (5.5%)
2.70	48.7	47.7 (– 2.0%)
3.24	59.0	57.3 (– 2.3%)
3.78	75.4	66.8 (– 16.4%)

Table 8 Energy contributions in crushing of square tube according to analytical model

Energy Source	Value [J]	Percentage of Total [%]
Total	3059	–
Delamination	8	0.3
Corner Splits	4	0.1
Shearing	2436	79.6
Friction	612	20.0

also reported as a percentage of the total energy dissipation. Based on to the analytical model, the delaminations and the corner splits are negligible with respect to the friction and shearing energy, where the latter two make up for 99% of the total energy absorption.

A sensitivity analysis has been performed, to investigate the implication of the assumptions of the unknown variables in the analytical model. It is found that when changing the Mode I interlaminar fracture toughness to 2 N/mm, which is considered to be a high value [14], the mean crushing load only changes with 1%. Altering the length of the corner split has an even lesser influence. The wedge angle does have a larger impact on the analytical mean crushing load (±10%). However, reference research shows that the wedge angle is around the assumed value of 45° [42], and is therefore deemed valid.

Tables 6 and 7 show that the suggested model is able to estimate the mean crushing load for the studied absorbers, provided that the absorbers are not susceptible to geometric instabilities. The obtained errors for the stable absorbers are below 10%, which is accurate, given the variable nature of the crushing phenomenon.

The energy absorption values reported in Table 8 show that shearing and friction are the main contributors to the energy dissipation, accounting for 99% of the total energy absorption, while the other phenomena are negligible. This means that the applicability of the analytical model can be broadened, by omitting the minor energy dissipating phenomena. For example, the number of corner splits does not need to be determined. As such, the analytical model can be used to determine the mean crushing load of round-like absorbers, where the determination of the corner splits is more difficult, due to the lack of stress concentrations. Moreover, the delamination energy can be omitted, eliminating the necessity to know the Mode I fracture toughness of the material.

Consequently, the main parameters that influence the mean crushing load are the thickness of the laminate, its out-of-plane shear strength and the total perimeter of the specimen. These can thus be tailored to achieve the desired crushing behavior.

3.2 Fuselage structure

Three different configurations are studied in the fuselage analysis. These are referred to as follows:

- STUNNING: this entails the original subfloor of the Next Generation Multifunctional Fuselage Demonstrator, which is characterized by the C-shaped struts.
- Benchmark: this is equal to the STUNNING fuselage, but has no struts or absorbers in the keel section. This fuselage serves as a reference to study the change in load and energy absorption of the fuselage when absorbers or struts are included.
- Square Tube Fuselage: this is the configuration where the benchmark fuselage is augmented with a square tube absorber, where the weight of the absorbers is equal to the C-struts.

The crash load and energy absorption for the three fuselage configurations are reported in Fig. 6. Figure 6a depicts the crash loads, which are extracted as a reaction force of the loading plate. Figure 6b shows the energy absorption during the crash. Note that the load is filtered using the built-in SAE filter with a cut-off frequency of 180 Hz.

The figures enable a comparison between the studied fuselages. The blue continuous line in Fig. 6 shows how the load drops once the frames have collapsed at 20 ms, after which a small peak is observed at 25 ms, which is

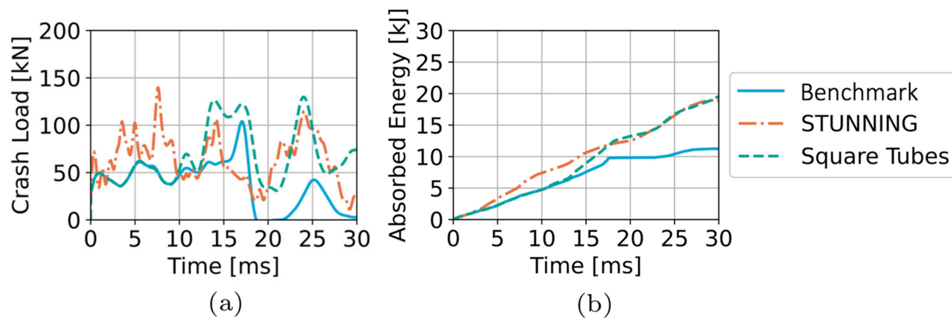

Fig. 6 Comparison for the different fuselage configurations: **a** Crash load–time curves; **b** Absorbed energy–time curves

when the crushing plate comes into contact with the hinge points of the frame, which in turn also collapse. The drop in load is accompanied by a plateauing behavior of the energy absorption. Here the difference between the fuselage section with no absorbers and the ones with the energy absorbers is clearly visible as the energy absorption of these fuselages continues to rise till the end of the simulation. The collapse of the C-strut is accompanied by a load drop toward the end of the simulation, depicted by the orange dash-dotted line. The square tube absorber, on the other hand, is still able to sustain load, meaning that the structural element can accommodate more energy absorption.

When studying the fuselage section, the loads and energy absorption are of key interest once the desired crash kinematics is achieved. Here the difference between the fuselage with no absorbers and the one with square tube absorbers can be clearly seen, characterized by the plateau in the energy absorption on one side and a continuous increase on the other. There is a load drop in the STUNNING fuselage at the end of the simulation, as the struts collapsed; on the other hand, in the keel section with the square tube, the crushing load is sustained. This once more confirms the stability of the square tube absorber and its effectiveness as an energy absorber.

Figure 7 reports a detail of the deformation of the STUNNING configuration. It is possible to note how the connection between the different parts influences the crash kinematics. The rigid attachment of the strut obstructs the desired crushing of the absorber, leading to failure in the middle of the structural element.

To study the Square Tube Fuselage, the material and geometry of the tube are changed such that the material data reported in Table 4 are used, and the cross section of the absorber is such that its weight is equal to the original C-strut. Furthermore, to promote the desired crash kinematics, the connection of the absorber with the frame is removed, so that the lower end of the absorber is free. This modeling choice promotes the formation of a stable crush

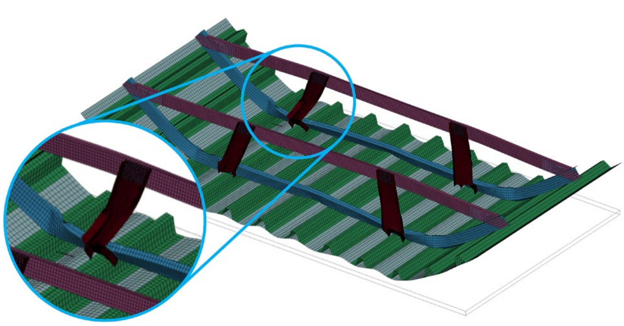

Fig. 7 Failure of the energy absorber in proximity of its connection to the frame in the fuselage section with the original STUNNING configuration

frond. A simplified payload mass of 120 kg is also introduced in the simulation. The deformations obtained at different time instances are reported in Fig. 8, where the payload mass is not shown to better highlight the deformation of the structure.

The deformation of the benchmark fuselage section is similar to the one reported in Fig. 8, without the presence of the absorbers. The deformation mainly occurs in the frames, while the skin-stringer configuration remains largely intact, but the absorbed energy is significantly lower, as shown in Fig. 6.

A flow diagram of the suggested method is reported in Fig. 9. At first, the fuselage with no absorbers and the absorbers are studied in an isolated manner. The fuselage is studied using finite element code, to obtain the benchmark behavior, yielding an estimation for the crushing load and the energy absorption. With that knowledge, an absorber is designed using the analytical model, which can be tailored to achieve the desired mean crushing load. Combining the absorber and the benchmark fuselage leads to the fuselage with the absorbers, the augmented fuselage, for which the mean crushing load and total energy absorption can be determined. When these parameters are as desired, the design has to be verified using numerical simulations, whereas when one of the values is not as desired, the absorber is to be redesigned using the analytical model. This process is repeated till the desired behavior is obtained. Validation steps may be required to ensure the validity of the numerical models.

The added value of the analytical model is that it provides a clear estimation of the influence of the different variables which can be altered to obtain the desired load and energy absorption. This greatly speeds up the design iterations as the dependency on time consuming numerical simulations is reduced. A single iteration of the absorber using finite elements is shown to take three to four hours, whereas the analytical analysis only takes milliseconds.

When using the suggested method in the current study, the benchmark fuselage section has an energy absorption of 11.2 kJ, while the energy absorption by the four square tubes is computed to be of 24.5 kJ. By combining the energy absorption of the fuselage with no absorbers and the estimated energy of the absorbers, a theoretical total energy absorption of 35.7 kJ is obtained. The energy absorption extracted from the simulation is of 29.9 kJ, which leads to a discrepancy of 20%. Given the complex nature of the problem, this falls within the desired margin. The discrepancy may arise from different aspects. First, introducing the absorbers may slightly change the crash kinematics of the fuselage, leading to different energy absorption levels. Moreover, while from Fig. 8, the absorbers seem to behave as desired, other phenomena may lead to sub-optimal energy absorption. Finally, but most importantly, the analytical model is not

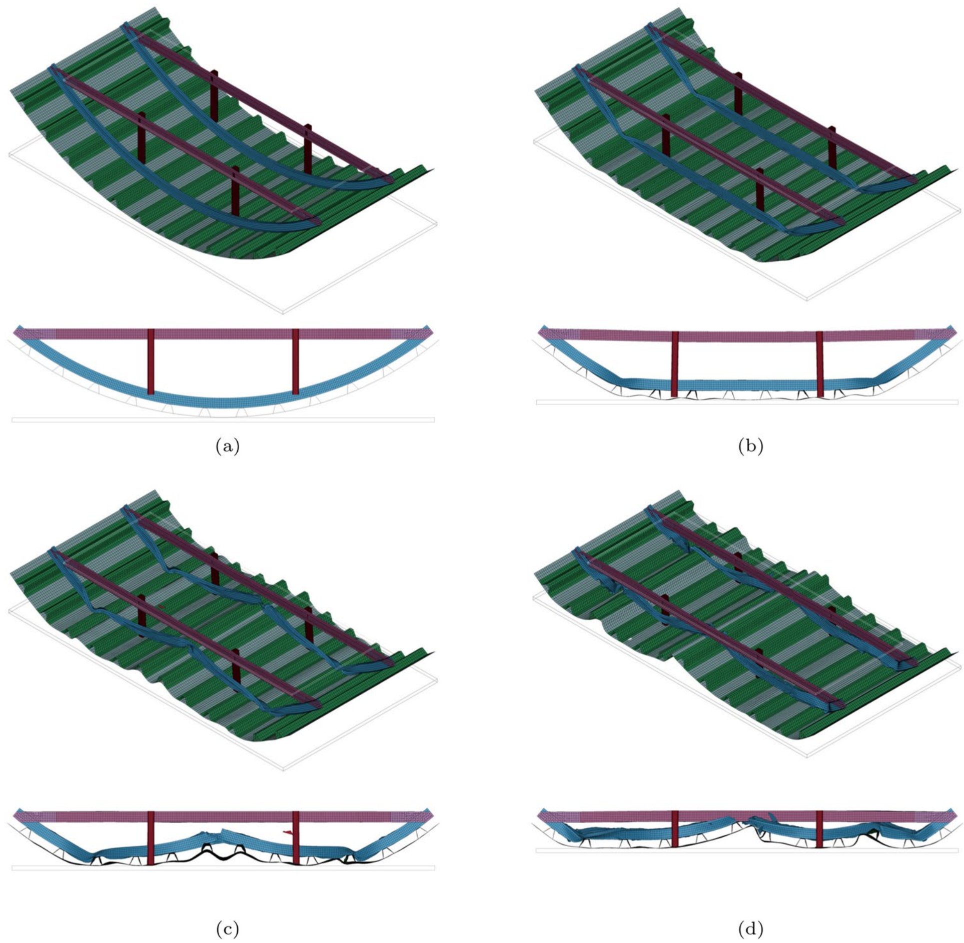

Fig. 8 Deformed states of the fuselage section with square tube absorbers and no connections to the frame: **a** time = 0.0 ms, **b** time = 10.0 ms, **c** time = 20.0 ms, **d** time = 30.0 ms

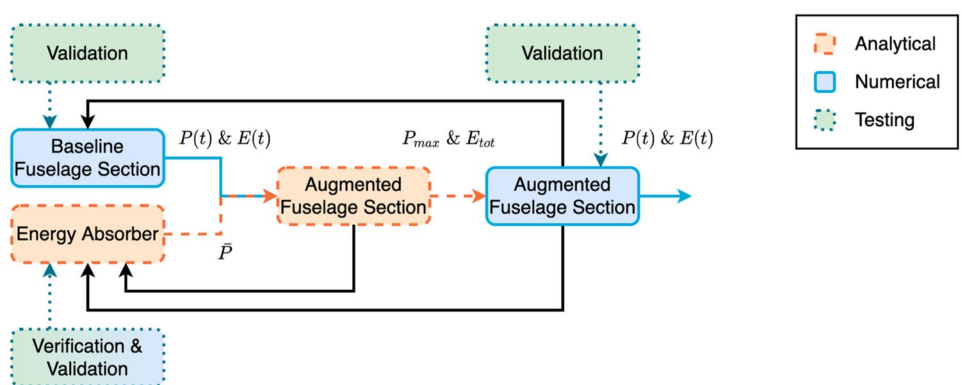

Fig. 9 Schematic representation of the analytical–numerical approach

perfectly accurate, thus a large part of the inconsistency is most likely due to the inaccuracy of the analytical model. Nevertheless, the tool provides direct insight into which variables influence the crush performance of a composite energy absorber, thus aiding during the preliminary design of an aircraft fuselage.

4 Conclusions

This paper develops an analytical–numerical method which can be implemented during the preliminary design for crashworthiness of an aircraft structure. Current methods entail the use of complex finite element simulations, which can only be performed in final design stages as they require a certain maturity of the design. Consequently, there is low flexibility when the design needs to be altered to account for the crashworthiness requirements, leading to a sub-optimal product.

Therefore, first, an analytical model is studied that estimates the mean crushing load of composite energy absorbers. The analytical model is verified using finite element simulations performed in LS-Dyna, which in turn are validated using test data. It predicts the crushing load of a square composite tube with an error of 10%.

The square composite absorbers are then integrated into the keel section of the Next-Generation Multifunctional Fuselage Demonstration as developed by the Clean Sky 2 STUNNING project, made from thermoplastic composites. It is found that the structure, when subjected to crash loading, is characterized by the formation of hinge points in the fuselage's frame. During the initial stages of the simulation, the fuselage with and without square tube absorbers behave in a similar fashion. However, in the final stages, characterized by the deployment of the absorbers, a clear difference can be noted in the load experienced by the fuselage section, leading to higher overall energy absorption. Indeed, the square tube absorbers are fully crushed as desired, maximizing the energy absorption.

The suggested analytical–numerical method can be used to estimate the crashworthiness behavior of the lower section of an aircraft fuselage. This is done by starting with the crush behavior of a benchmark fuselage obtained from numerical simulations. Based on the benchmark behavior, a composite energy absorber can be designed with the analytical method. This process may be repeated iteratively until the load and energy absorption requirements are met.

The suggested method provides direct insight into the design variables that influence the crashworthiness behavior, reducing the need for time-consuming finite element simulations during the preliminary design stages of an aircraft fuselage. This enables engineers to account for crashworthiness during the preliminary design stages, yielding a more synergistic, and thus lightweight design.

Acknowledgements The work described in this paper received co-funding from the Clean Sky 2 Joint Undertaking (JU) under grant agreement No 945583 (project STUNNING). The JU receives support from the European Union's Horizon 2020 research and innovation programme and the Clean Sky 2 JU members other than the Union.

Author contributions V.P.'s contribution consists of the conceptualization and development of the methodology, in the software development and data curation, and in writing the original draft of the manuscript. C.B.'s contribution consists of the conceptualization and development of the methodology, in reviewing and editing the manuscript, in the supervision of the research activity, and in the acquisition of the financial support for the project leading to this publication.

Data availability No datasets were generated or analyzed during the current study.

Declarations

Conflict of interest No potential conflict of interest was reported by the authors.

References

1. Airworthiness standards: Transport category airplanes, 14 CFR § 25 (2011)
2. Hull, D.: A unified approach to progressive crushing of fibre-reinforced composite tubes. Compos. Sci. Technol. **40**(4), 377–421 (1991). https://doi.org/10.1016/0266-3538(91)90031-J
3. Lukaszewicz, D.H.J.A.: Automotive composite structures for crashworthiness. Adv. Compos. Mater. Autom. Appl. (2013). https://doi.org/10.1002/9781118535288.ch5
4. Bisagni, C.: Experimental investigation of the collapse modes and energy absorption characteristics of composite tubes. Int. J. Crashworth. **14**(4), 365–378 (2009). https://doi.org/10.1080/13588260902792954
5. Falzon, B.G.: Computational modelling of the crushing of carbon fibre-reinforced polymer composites. Philos. Trans. Royal Soc. A (2022). https://doi.org/10.1098/rsta.2021.0336
6. Sokolinsky, V.S., Indermuehle, K.C., Hurtado, J.A.: Numerical simulation of the crushing process of a corrugated composite plate. Compos. Part A Appl. Sci. Manuf. **42**(9), 1119–1126 (2011). https://doi.org/10.1016/j.compositesa.2011.04.017
7. Zhu, G., Sun, G., Li, G., Cheng, A., Li, Q.: Modeling for CFRP structures subjected to quasi-static crushing. Compos. Str. **184**, 41–55 (2018). https://doi.org/10.1016/j.compstruct.2017.09.001
8. Zhao, X., Zhu, G., Zhou, C., Yu, Q.: Crashworthiness analysis and design of composite tapered tubes under multiple load cases. Compos. Str. **222**, 110920 (2019). https://doi.org/10.1016/j.compstruct.2019.110920
9. Lombarkia, R., Gakwaya, A., Nandlall, D., Dano, M.L., Lévesque, J., Benkhelifa, A., Vachon-Joannette, P., Gagnon, P.: A mesomechanical material model describing a crash behavior of 2d plain weave fabric composites. CEAS Aeronaut. J. **12**, 147–171 (2021). https://doi.org/10.1007/s13272-020-00488-1
10. Zhan, B., Sun, L., Huang, B.: Progressive failure prediction of FRP tubes by modified damage model. Int. J. Crashworth. **23**(6), 593–604 (2018). https://doi.org/10.1080/13588265.2017.1368118
11. Cherniaev, A., Butcher, C., Montesano, J.: Predicting the axial crush response of CFRP tubes using three damage-based constitutive models. Thin-Walled Str. **129**, 349–364 (2018). https://doi.org/10.1016/j.tws.2018.05.003
12. Costa, S., Zrida, H., Olsson, R., Herraez, M., Östlund, R.: A unified physically-based finite deformation model for damage growth in composites. Compos. Part A: Appl. Sci. Manuf. (2022). https://doi.org/10.1016/j.compositesa.2022.107103
13. Boria, S., Pettinari, S., Giannoni, F.: Theoretical analysis on the collapse mechanisms of thin-walled composite tubes. Compos. Str. **103**, 43–49 (2013). https://doi.org/10.1016/j.compstruct.2013.03.020
14. Hussein, R.K., Ruan, D., Lu, G.: An analytical model of square CFRP tubes subjected to axial compression. Compos. Sci. Technol. **168**, 170–178 (2018). https://doi.org/10.1016/j.compscitech.2018.09.019
15. Riccio, A., Saputo, S., Sellitto, A., Di Caprio, F., Di Palma, L.: A numerical-experimental assessment on a composite fuselage barrel vertical drop test: induced damage onset and evolution.

Compos. Str. (2020). https://doi.org/10.1016/j.compstruct.2020.112519
16. Paz Mendez, J., Díaz Garcia, J., Romera Rodriguez, L.E., Teixeira-Dias, F.: Crashworthiness study on hybrid energy absorbers as vertical struts in civil aircraft fuselage designs. Int. J. Crashworth. **25**(4), 430–446 (2020). https://doi.org/10.1080/13588265.2019.1605723
17. Tay, Y.Y., Flores, P., Lankarani, H.: Crashworthiness analysis of an aircraft fuselage section with an auxiliary fuel tank using a hybrid multibody/plastic hinge approach. Int. J. Crashworth. **25**(1), 95–105 (2020). https://doi.org/10.1080/13588265.2018.1524547
18. Caputo, F., Lamanna, G., Perfetto, D., Chiariello, A., Di Caprio, F., Di Palma, L.: Experimental and numerical crashworthiness study of a full-scale composite fuselage section. AIAA J. **59**(2), 700–718 (2021). https://doi.org/10.2514/1.J059216
19. Cronkhite, J., Berry, V.: Crashworthy airframe design concepts - fabricating and testing. NASA Techn. Rep. 19820025859 (1982)
20. Ren, Y., Xiang, J., Zheng, J., Luo, Z.: Crashworthiness analysis of aircraft fuselage with sine-wave beam structure. Chinese J. Aeronaut. **29**(2), 403–410 (2016). https://doi.org/10.1016/j.cja.2016.02.002
21. Sashikuma, H., Isoe, A., Yamaoka, T., Katayama, N., Hayashi, T., Akaso, T., Kumakura, I., Minegishi, M., Iwasaki, K., Shoji, H., Yoshimoto, N., Terada, H.: Vertical drop test of a transport fuselage section. In: World Aviation Congress & Exposition. SAE Int. (2002). https://doi.org/10.4271/2002-01-2997
22. Abramowitz, A., Smith, T., Vu, T., Zvanya, J.: Vertical drop test of a narrow-body transport fuselage section with overhead stowage bins. World Aviat. Congress Expos. (2002). https://doi.org/10.4271/2002-01-2995
23. Gransden, D., Alderliesten, R.: Development of a finite element model for comparing metal and composite fuselage section drop testing. Int. J. Crashworth. **22**(4), 401–414 (2017). https://doi.org/10.1080/13588265.2016.1273987
24. Song, Y., Horton, B., Perino, S., Thurber, A., Bayandor, J.: A contribution to full-scale high fidelity aircraft progressive dynamic damage modelling for certification by analysis. Int. J. Crashworth. **24**(3), 243–256 (2019). https://doi.org/10.1080/13588265.2018.1424683
25. Schwinn, D., Kohlgrüber, D., Scherer, J., Siemann, M.: A parametric aircraft fuselage model for preliminary sizing and crashworthiness applications. CEAS Aeronaut. J. **7**(3), 357–372 (2016). https://doi.org/10.1007/s13272-016-0193-4
26. Schatrow, P., Waimer, M.: Crash concept for composite transport aircraft using mainly tensile and compressive absorption mechanisms. CEAS Aeronaut. J. (2016). https://doi.org/10.1007/s13272-016-0203-6
27. Federal Register, O.: Special Conditions: Boeing Model 787-8 Airplane; Crashworthiness, 72 FR 54531. (Accessed: 25.09.2020) (2007). https://www.govinfo.gov/app/details/FR-2007-09-26/E7-18942
28. Federal Register, O.: Special Conditions: Airbus A350-900 Airplane; Crashworthiness, Emergency Landing Conditions, 79 FR 43237. (Accessed: 25.09.2020) (2014). https://www.govinfo.gov/app/details/FR-2014-07-25/2014-17574
29. Courteau, M.: Investigating the crashworthiness characteristics of carbon fiber/epoxy tubes. PhD thesis, Department of Mechanical Engineering, University of Utah (2011)
30. Jiang, H., Ren, Y., Gao, B., Xiang, J.: Numerical investigation on links between the stacking sequence and energy absorption characteristics of fabric and unidirectional composite sinusoidal plate. Compos. Str. **171**, 382–402 (2017). https://doi.org/10.1016/j.compstruct.2017.03.047
31. Boria, S., Obradovic, J., Belingardi, G.: Experimental and numerical investigations of the impact behavior of composite frontal crash structures. Compos. Part B Eng. **79**, 20–27 (2015). https://doi.org/10.1016/j.compositesb.2015.04.016
32. Charoenphan, S., Bank, L.C., Plesha, M.E.: Progressive tearing failure in pultruded composite material tubes. Compos. Str. **63**(1), 45–52 (2004). https://doi.org/10.1016/S0263-8223(03)00130-2
33. Chambe, J., Bouvet, C., Dorival, O., Ferrero, J.: Energy absorption capacity of composite thin-wall circular tubes under axial crushing with different trigger initiations. J. Compos. Mater. **54**(10), 1281–1304 (2020). https://doi.org/10.1177/0021998319877221
34. LS-DYNA: Keyword User's Manual vol. 1. Livermore Software Technology Corporation (LSTC), (2023)
35. Pinho, S.T., Camanho, P.P., Moura, M.F.: Numerical simulation of the crushing process of composite materials. Int. J. Crashworth. **9**(3), 263–276 (2004). https://doi.org/10.1533/ijcr.2004.0287
36. Schön, J.: Coefficient of friction of composite delamination surfaces. Wear **237**(1), 77–89 (2000). https://doi.org/10.1016/S0043-1648(99)00315-4
37. Fasanella, E., Jackson, K.: Best practices for crash modeling and simulation. NASA Techn. Rep. 20020085101 (2002)
38. Transport Aircraft Crashworthiness and Ditching Working Group: Transport Aircraft Crashworthiness and Ditching Working Group Report to FAA vol. 3743. Federal Aviation Association (2018)
39. Lian, E., Lovingfoss, R., Tanoto, V.: Medium toughness PAEK thermoplastics Toray (formerly TenCate) Cetex TC1225 (LM PAEK) T700GC 12K T1E unidirectional tape 145 gsm 34% RC qualification material property data report. Wichita State University, National Center for Advanced Materials Performance (CAM-RP-2019-036 Rev N/C) (2020)
40. Zhao, T., Rans, C., Fernandez Villegas, I., Benedictus, R.: On sequential ultrasonic spot welding as an alternative to mechanical fastening in thermoplastic composite assemblies: A study on single-column multi-row single-lap shear joints. Compos. Part A Appl. Sci. Manuf. **120**, 1–11 (2019). https://doi.org/10.1016/j.compositesa.2019.02.013
41. Dooren, K.S., Bisagni, C.: Design and analysis of thermoplastic welded stiffened panels in post-buckling. 36th Technical Conference of the American Society for Composites 2021: Composites Ingenuity Taking on Challenges in Environment-Energy-Economy, ASC 2021 1, 406–417 (2021)
42. Mamalis, A.G., Manolakos, D.E., Demosthenous, G.A., Ioannidis, M.B.: The static and dynamic axial crumbling of thin-walled fiberglass composite square tubes. Compos. Part B Eng. **28**(4), 439–451 (1997). https://doi.org/10.1016/S1359-8368(96)00066-2